Clim Dyn
DOI 10.1007/s00382-009-0596-6

The dynamics of the Indian Ocean sea surface temperature forcing of Sahel drought

Jian Lu

Received: 29 February 2008 / Accepted: 11 May 2009

Abstract Given the pronounced warming in the Indian Ocean sea surface temperature (SST) during the second half of the twentieth century and the empirical relationship between the Indian Ocean SST and Sahel summer precipitation, we investigate the mechanisms underlying this relationship using the GFDL atmospheric model AM2.0 to simulate the equilibrium and transient response to the warming of the Indian Ocean. Equatorial wave dynamics, in particular the westward propagating equatorial Rossby waves, communicates the signal of tropospheric warming and stabilization from the Indian Ocean to the African continent. The stabilization associated with the Rossby wave front acts to suppress the convection. Feedbacks with local precipitation and depletion of moisture amplify the dynamically induced subsidence. While this stabilization mechanism is expected to operate in climate change response, the future prospects for the Sahelian climate under global warming are complicated by the intricate sensitivities to the SSTs from different ocean basins and to the direct radiative forcing of greenhouse gases.

1 Introduction

The Sahel, the transition zone between the Sahara desert and the tropical rainforest of Central Africa and Guinean Coast underwent a severe drying trend from the 1950s to the 1980s, one of the most devastating and extensively studied droughts in modern climate variability. The Sahelian monsoon system is very sensitive to the worldwide distributions of sea surface temperatures (SSTs). A body of observational and model studies associated the dry condition of the Sahel to warm SSTs in the south Atlantic and the Gulf of Guinea (Lamb 1978; Hastenrath 1990; Vizy and Cook 2001, 2002); the interhemispheric SST contrast, in particular the north-south SST dipole over the Atlantic (Hoerling et al. 2006; Folland et al. 1986; Palmer 1986; Rowell et al. 1995; Fontaine et al. 1998; Rotstayn and Lohmann 2002); the SST warming over the equatorial east Pacific (Janicot et al. 1996, 2001; Nicholson and Kim 1997); and the SST warming over the Indian Ocean (Shinoda and Kawamura 1994; Bader and Latif 2003; Giannini et al. 2003).

The global SST pattern (see Fig. 9) associated with drought at decadal and longer time scales is characterized by a global inter-hemispheric SST contrast, with significant warming over the subtropical south Atlantic and south Indian Ocean, cooling over the northern north Atlantic and mid-latitude Pacific, and tropical warming over the eastern Pacific and Indo-western Pacific. The connection of the inter-hemispheric SST contrast to the Sahel drought has been well established (e.g., Folland et al. 1986, 1998; Rowell et al. 1995; Rotstayn and Lohmann 2002; Hoerling et al. 2006) and there is continuing progress in understanding the dynamics underlying this response(see Kang et al. 2008 and references therein).

The connection of the Indian ocean to the drought is relatively less well established and the dynamics of this connection is not well understood. The question of the Indian Ocean's role in Sahel drought is particularly intriguing because there has been a pronounced multi-decadal warming trend of the Indian Ocean during the

J. Lu
George Mason University, Fairfax, VA, USA

J. Lu (✉)
Center for Ocean-Land-Atmosphere Studies,
4041 Powder Mill Rd, Suite 302,
Calverton, MD 20705-3106, USA
e-mail: jianlu@cola.iges.org

Published online: 31 May 2009

second half of the twentieth century (Levitus et al. 2000) and this warming is consistent with the expected greenhouse gas (GHG) signal (Hurrell et al. 2004; Knutson et al. 1999, 2006). Therefore, understanding the role and the dynamical mechanisms of the Indian Ocean forcing for the Sahel drought in the twentieth century should have relevance to the future projection of Sahel climate with increasing greenhouse gas forcing. It is the Indian Ocean connection on which we focus here, building specifically on the work of Lu and Delworth (2005) with the GFDL AM2.0 model.

Previous studies have identified some statistical relationship between the Indian Ocean SST and the Sahel precipitation on interdecadal time scales in observations (Hastenrath and Wolter 1992; Shinoda and Kawamura 1994; Giannini et al. 2003) and coupled model simulations (Biasutti et al. 2008). For example, based on simulations by NSIPP1 (version 1 of the AGCM developed at NASA's Goddard Space Flight Center) with the observed history of the twentieth century global SSTs, Giannini et al. (2003, 2005) proposed that the interdecadal variability of the Sahel rainfall is forced by warm waters surrounding the African continent, especially the Indian Ocean SST. The hypothesis for significant Indian Ocean forcing for Sahel drought gains some support from the experiments with the ECHAM4.5 model (Bader and Latif 2003, personal communication). These authors found a wide-spread drying over most of the Sahel forced by 1 K uniform warming of the Indian Ocean SST, a pattern closely resembling the response of GFDL AM2.0 model to the same Indian Ocean warming. In another regional modeling study, Hagos and Cook (2008) also identified the Indian Ocean as the primary player for the epoch of drought during the 1980s. The results of Hoerling et al. (2006) are somewhat different, however. Using five different AGCMs with observed global SST forcing, Hoerling et al. found that the multi-model ensemble mean successfully reproduced many aspects of the drying trend in Sahelian summer. However, an ensemble of 40 integrations (20 using NCAR's CAM-2, 20 using the NSIPP1 model) forced by an idealization of the Indian SST trend pattern simulates rainfall anomalies with little drying poleward of 15°N and instead an increase across the central and eastern Sahel within 15–20°N during July–August–September (their Fig. 7), a result that does not support the hypothesis of Indian Ocean forcing proposed by Giannini et al. (2003).

The GFDL coupled models (CM2.0 and CM2.1), which use AM2.0 and AM2.1 as their atmospheric components, both project a very strong drying future for the Sahel climate under different warming scenarios (Held et al. 2005). They are outliers in this respect among the models in the CMIP3 database (Biasutti et al. 2008). But despite this outlier status, both CM2 models, forced with the observed GHG and aerosol forcing during the twentieth century, are able to reproduce many aspects of the observed drying over the Sahel. The atmospheric components of both models, when run over observed global SSTs, provide realistic simulations of the pattern of the drying trend (Lu and Delworth 2005; Held et al. 2005). Given the quality of their twentieth century simulations, here we use the AM2 to revisit the role of the Indian Ocean in the late twentieth century Sahel drought and to elucidate the dynamical processes that lead to the Sahelian response. The model to be used intensively in this study is the AM2.0, and due to its being outlier among other climate models, and because there has been discussion of some model deficiencies (e.g., Cook and Vizy 2006), we include here some further analysis of the tropical circulation and hydrology simulated by AM2.0, before proceeding to analyze its response to Indian Ocean SSTs.

According to Giannini et al. (2008), the effects of the Indian Ocean on African climate are most easily visualized as due to a stabilization of the African atmosphere associated warming of the troposphere, but moisture supply can also be modified by the circulations induced by anomalous convection to the east of the continent. To aid in sorting out causal relationships and distinguishing between these two perspectives, in addition to the familiar prescribed SST anomaly simulations, we follow a methodology used by Lintner and Chiang (2006) in a related context. We consider a large ensemble of simulations in which we change the SSTs in the Indian Ocean abruptly and study the time evolution of the response throughout the tropics and over Africa in particular. Lintner and Chiang (2006) focus on the equatorially trapped Kelvin wave-like component east of the forcing, while here we focus on the off-equatorial Rossby wave-like response west of the forcing.

The choice of AM2.0 and our experimental design are discussed in Sect. 2. Section 3 assesses the AM2.0 performance on the climatology of precipitation and circulations over the tropical Atlantic-Africa sector. The reproduction of multidecadal variability in the twentieth century Sahelian precipitation is examined in Sect. 4. In Sect. 5, we describe the time-dependent response of AM2.0 to perturbations in Indian Ocean SSTs. Section 6 summarizes the results and discusses future research needs and prospects of Sahelian climate.

2 Model and experiment design

2.1 AM2

The basic tool for this study is the general circulation model constructed by the GFDL Global Atmospheric Model Development Team (GAMDT). The configuration

of this atmosphere-land model (referred as AM2.0 hereafter) and its performance in replicating various aspects of the atmospheric climate have been reported in detail by GAMDT (2004). The model contains a prescribed aerosol distribution that does not interact with the model clouds (so there are no indirect aerosol effects). The aerosols include a dust component that is also prescribed, so dust over Africa and the Atlantic does not respond to African climate. The terrestrial component of the model, LM2, is based on the Land Dynamics model described by Milly and Shmakin (2002). The soil and vegetation dependent parameters are spatially varying but fixed in time. Therefore, vegetation feedback is not represented in the AM2/LM2 model.

A different version of the atmospheric component model, AM2.1, has been also been studied extensively. The configuration of AM2.1 is presented in detail in Delworth et al. (2006), where the relative merits of the coupled models based on these atmospheric components are discussed. Briefly stated, CM2.1 is found to be more realistic in extratropical latitudes, especially because of improved Southern Hemispheric winds and smaller temperature biases in the subpolar North Atlantic and Pacific. However, CM2.0 has some more realistic features in the tropics, owing in part to the fact that CM2.1's ENSO variability in unrealistically strong. Gleckler et al. (2008) ranks CM2.0 as one of those having the most realistic climatological tropical precipitation pattern among the CMIP3 participating models. Given the somewhat more realistic tropical simulation in CM2.0, we focus on AM2.0 in this study.

2.2 Experiments setup

Two types of experimentation strategies are employed. In one, the full history of monthly SSTs is used as the boundary condition for an ensemble of experiments; these runs will be referred to as full SST runs. For the full SST runs, three sets of experiments are carried out with AM2.0: Global ocean and global atmosphere (GOGA) experiment that runs over the full history of the global SST and sea ice from 1950 to 2000; Topical ocean and global atmosphere, or TOGA (Indo-Pacific oceans and global atmosphere, IPGA) experiment differs from GOGA in that the SSTs vary only within the tropical band between 30°S and 30°N (the tropical Indian and Pacific oceans within 30°S–30°N), elsewhere being specified as seasonally evolving climatology. Each set of experiment consists of 10 realizations, each differing only in the atmospheric and land initial conditions. The SST and sea ice data used were provided by Jim Hurrell at NCAR and based on the HadISST dataset (Rayner et al. 2003). The full SST experiments simulate the full history of climate variation, facilitating direct year-to-year comparison with the observations.

In another, SST anomalies are superimposed upon the seasonally evolving climatology of the global SST to drive an ensemble of runs for only a few months from May 1st to September 30th (referred to as MS experiments hereafter) and the difference from the ensemble simulations driven solely by the SST climatology (control runs) gives the response to the SST perturbations. As the full SST experiment, the MS experiment comprises 10 ensemble members too. This second strategy provides a computationally economical way to examine the model sensitivity to different SST patterns (e.g., Folland et al. 1986; Rowell 2003).

In order to estimate the role of the Indian Ocean SST in forcing the Sahel drying trend, first, JAS summer mean SSTs are regressed against the 5-year low-pass filtered time series of the observed Sahel Rainfall Index (SRI, areal weighted average of rainfall over 10–20°N, 20°W–40°E) during 1901–2002; then the regression loadings over the Indian Ocean basin associated with two standard deviation of SRI are added onto the SST climatology to drive an ensemble of MS experiments. This experiment will be referred to as IND-MS, henceforth. Similar experiments using the SST regression patterns over the Atlantic and Pacific oceans have been reported in Lu and Delworth (2005).

3 Validation of climatology

3.1 Precipitation

We first describe AM2.0's performance in reproducing the observed climatology based on the 51-year ensemble mean of the GOGA simulations. Figure 1a shows the July–August–September (JAS) summer mean rainfall and vertically integrated moisture transport. Compared to the observations (the CPC Merged Analysis of Precipitation, CMAP, Xie and Arkin 1997) shown in Fig. 1b, the AM2.0 can realistically simulate the spatial structure of the rainfall distribution over the tropical Atlantic and Africa, though the latter is slightly narrower and sharper than the observed. The model does not capture the precipitation maximum over the coastal area of Nigeria and Cameroon, a feature likely related to the local orography and not resolved by this $\sim$200 km resolution model. AM2.0 also gives a reasonable representation of Indian monsoon rainfall and the South Pacific Convergence Zone.

The simulated moisture flux implies three sources of moisture supply for the summer African rain belt: one from the tropical Atlantic coast; one from the Mediterranean, veering across the desert toward the northern fringe of rain belt; and another from the equatorial Indian Ocean. It is well known that the tropical easterlies from the south tropical Indian Ocean are steered clockwise by the eastern

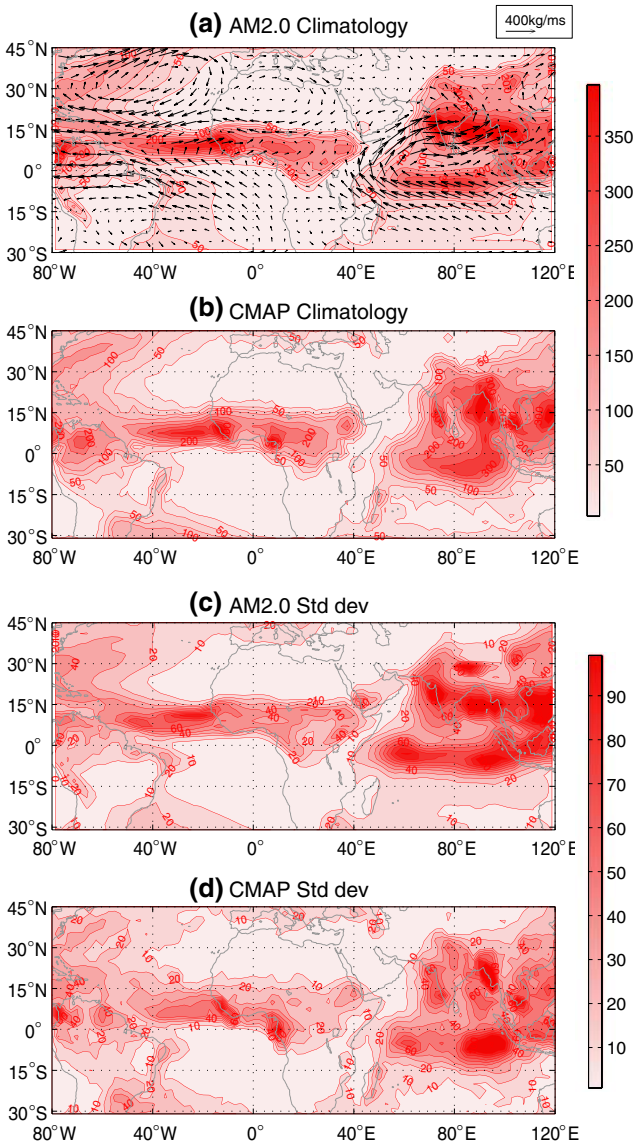

Fig. 1 Comparison of the observed (CMAP) and AM2.0 GOGA simulated climatology for mean and standard deviation of July–September precipitation. Unit is mm month^{-1} for both mean and standard deviation. Also plotted in panel (**a**) is the vertically integrated moisture flux

African highlands towards the India subcontinent, supplying moisture for the summer Indian monsoon. But it appears that some of the Indian Ocean moisture leaks inland toward the southeastern face of the African rain belt. The summer Sahel precipitation may be sensitive to the moisture supply from Indian Ocean, as suggested later by the Indian Ocean SST experiments. The overall spatial distribution of the variability, measured by the ensemble average of the standard deviation of the seasonal mean rainfall for each member of the ensemble, compares favorably to the observations (Fig. 1c, d). But the model underestimates the variability over the Guinean and Cameroon highlands and overestimates it over the southern tip of Red Sea.

It has long been observed that summer Sahel rainfall tends to be anti-correlated with the rainfall along the Gulf of Guinea coast (Nicholson and Palao 1993; Rowell et al. 1995) and the reproduction of the meridional dipole structure has been considered as a benchmark test for model's ability to correctly simulate the variability of the West African monsoon (Vizy and Cook 2001, 2002). To assess this capability, we apply Empirical Orthogonal Function (EOF) analysis to the catenated JAS rainfall time series of all the 10 members of GOGA experiment over tropical Africa (between 20°N and 20°S) as well as to the land precipitation data obtained from the Climate Research Unit (CRU) at the University of East Anglia (version CRU-TS_2.1, Mitchell and Jones 2005). As in the observations, the leading EOF mode has a dipole structure with wet condition over the whole swath of Sahel from the Atlantic coast to the coast of the Red Sea and dry condition near the Gulf of Guinea south of 10°N (Fig. 2a, c). The model ensemble mean leading principal component (PC) (Fig. 2e, solid black line) correlates with its observational counterpart (Fig. 2e, dashed black line) at 0.62, both showing a declining trend from 1960s to 1980s. EOF analysis on the African rainfall from a long integration running over repeating annual cycles of SST boundary conditions results in a similar leading EOF pattern as Fig. 2c, suggesting that the existence of the dipole mode is not dependent on the SST variabilities, and hence likely to be intrinsic to the tropical African land-atmosphere system. Similar conclusion was reached by conducting EOF on the deviation time series of the each member from the ensemble mean in NSSIP1 simulations (Giannini et al. 2005). The second EOF (Fig. 2b, d) bears a strong resemblance to EOF1 of African precipitation simulated by NSSIP1 (Giannini et al. 2003; 2005), wherein this mode was attributed to the SST variability near the Guinean Gulf, a variability associated with the Atlantic counterpart to the Pacific El Niño-Southern Oscillation (ENSO). The correlation between the ensemble mean and the observed PC2 is 0.60. Provided that the ensemble mean precipitation anomalies are SST-driven, these correlations between the modeled and observed PCs indicate substantial contributions from the oceanic forcing to the variability of the leading two EOF modes. The two leading modes jointly explain no more than 30% of the total variance in observations; whereas, they account for 57% of the total variance of the north African rainfall in the realizations of the GOGA simulations.

Figure 3 presents the seasonal evolution of the monthly climatological rainfall (contours) zonally averaged over the African land region between 12 and 34°E, along with the annual cycle of the net radiative forcing at the top of

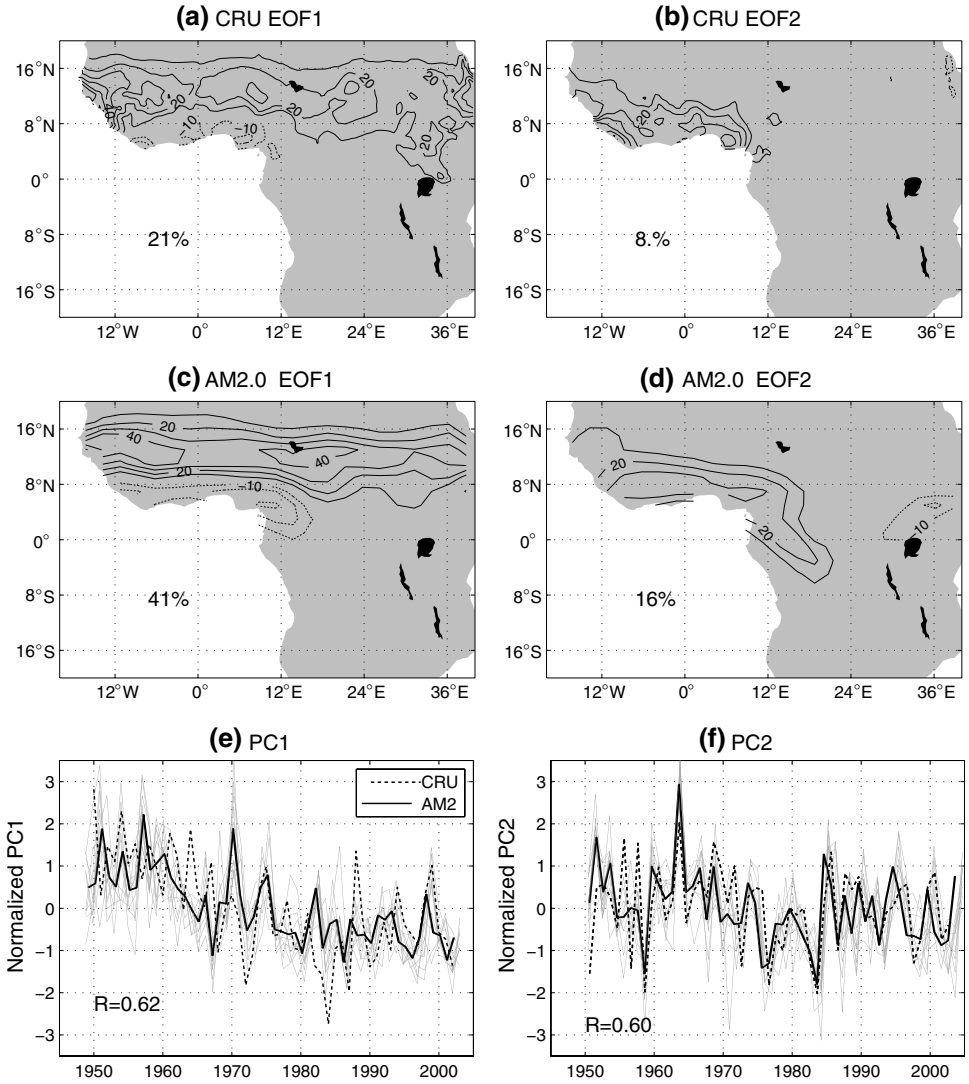

Fig. 2 Comparison between the observed (*top*) and AM2.0 GOGA simulated (*middle*) precipitation EOFs (dimensional pattern in unit of mm month^{-1}). The observations are based on CRU land precipitation data. The amplitudes of the EOFs are associated with one standard deviation of the corresponding principal component. The percentage indicates the variance explained by the corresponding EOF. Bottom panels compare the normalized time series of the observed (*dashed*) and modeled (*gray* for individual realizations and solid black for the ensemble mean) principal components for each EOF and the correlation coefficient between the modeled ensemble mean and observed time series is indicated

the atmosphere (TOA). Compared to the CMAP observations (Fig. 4a), the AM2.0 (Fig. 4b) has a relatively more accentuated African rainbelt. Otherwise, the model simulates a realistic seasonal migration of the rainbelt. In both model simulation and observation, the African rainbelt tends to follow the TOA radiation, with the former lagging the latter by about a month. The relationship between the precipitation and the TOA net radiative forcing suggests that convective precipitation is the result of energetical compensation for the net TOA energy gain by transporting moist static energy out of the area through overturning circulation. The associated ascending motion then determines the location of the rainbelt.

3.2 Circulation

Several circulation features are important to the tropical African rainfall and should be examined as a part of model evaluation. These include (i) equatorial westerly jet centered at 10°N, extending from the surface to 850 hPa level, bringing moisture from the Atlantic to the tropical north African coast, and creating a strong vertical and horizontal wind shear against the African Easterly Jet (AEJ); (ii) AEJ, centered at 15°N, 600 hPa, with its strengthening and southward shift associated with the drying of Sahel (Grist and Nicholson 2001; Nicholson and Grist 2001); and (iii) upper level Tropical Easterly Jet (TEJ) centered at 200 hPa level, it is also observed to influence the Sahel rainfall, but for reasons not well understood. Figure 4a, b depicts the zonal mean (from 20°W to 40°E) zonal wind over the tropical Africa from both ECMWF reanalysis (ERA40) and the GOGA simulations. AM2.0 reproduces these jets with realistic amplitude and position, except that the AEJ is slightly less accentuated than the observations.

Reproduction of the meridional circulation over the tropical Africa poses challenges to most atmosphere-ocean coupled models (Cook and Vizy 2006). In the ERA40

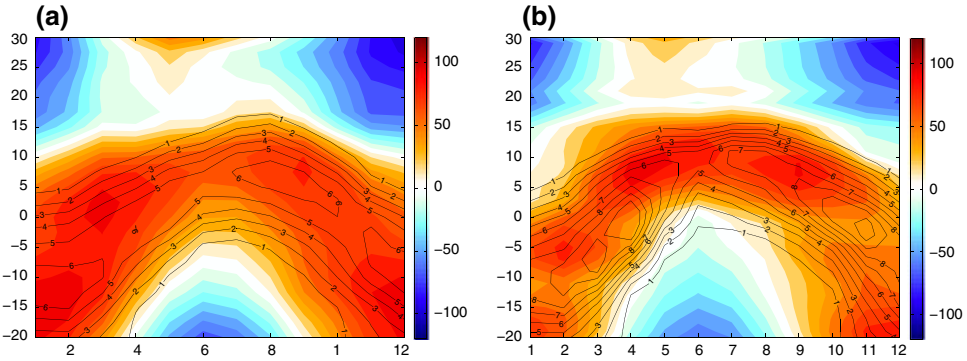

Fig. 3 Annual cycle of the zonally averaged (between 12 and 34°E), monthly mean precipitation (contours, unit is mm day^{-1}) and net radiative fllux (shading, unit is W m^{-2}) at the top of the atmosphere. (**a**) is calculated based on the CMAP precipitation data and ERBE radiation observations; (**b**) is calculated based on the ensemble mean of AM2.0 GOGA simulations

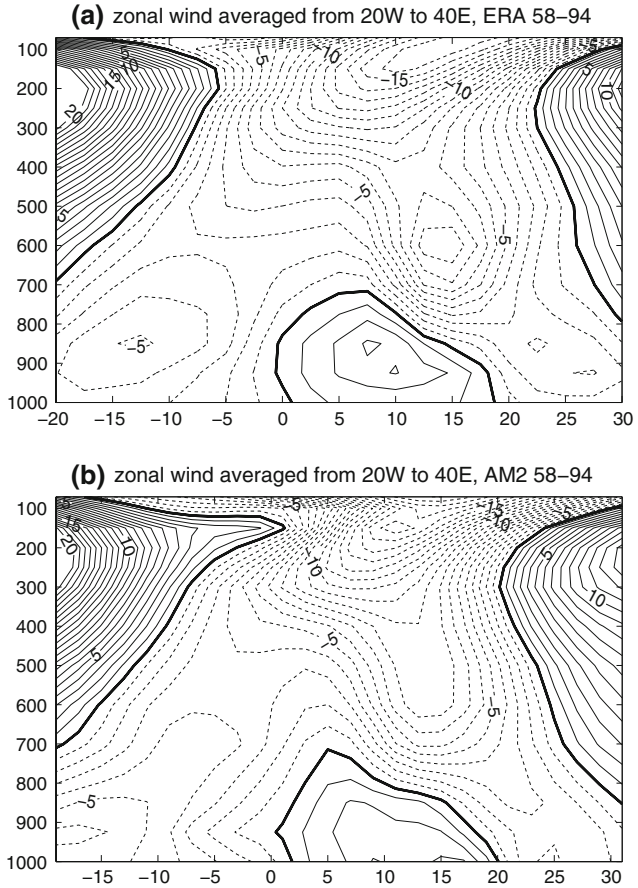

Fig. 4 JAS climatology of zonal mean zonal wind averaged between 20°W and 40°E over the tropical Africa using (**a**) observations based on ECMWF reanalysis from 1958 through 1994; (**b**) simulation by AM20 from 1958 through 1994. Counter interval is 1 m s^{-1}

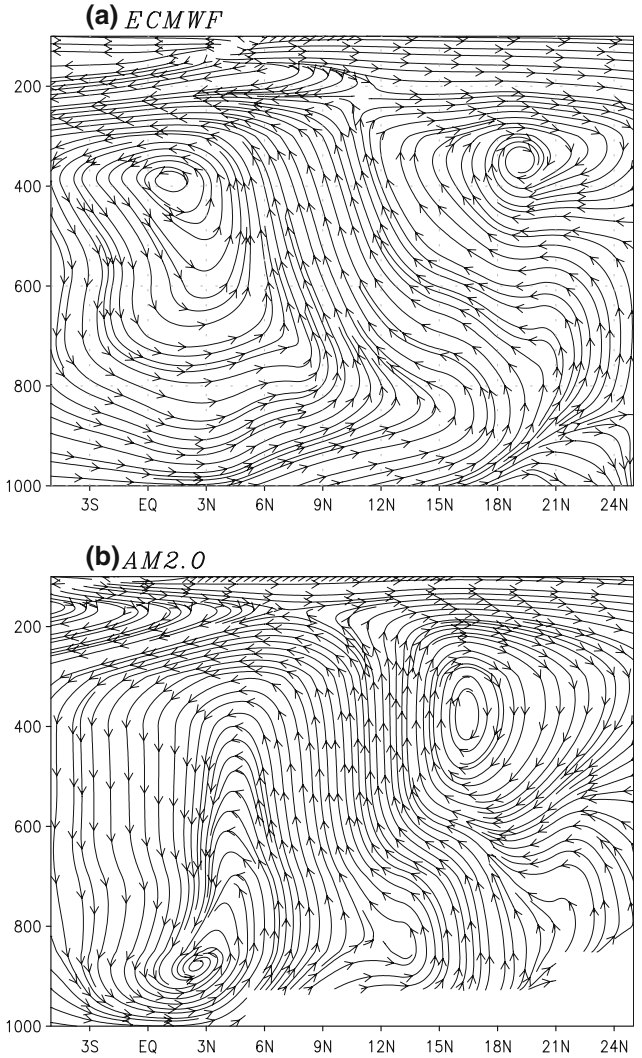

Fig. 5 Similar to Fig. 5 but for latitude-height cross-section of streamlines for v and $-\omega$ fields along 5°E. The vertical scale of ω is arbitrary

reanalysis (Fig. 5a), northward low-level monsoon flow crosses the Guinean coast and penetrates well onto the continent, as far north as 20°N, the northern edge of the African rain belt. Much of this onshore flow feeds into the deep convection between 5°N and 10°N. The flow that reaches further north converges with the northerly flow from Sahara and rises over the continental thermal low near 20°N. The rising motion is associated with the shallow convection driven by the hot and dry surface during the boreal summer. Barring moisture supply, the dry convection can not penetrate deep into the troposphere and the rising flow turns southward near mid-troposphere and feeds

into the deep convection further south. Thus, a strong northerly flow results near 600 hPa between 10°N and 20°N and the Coriolis force acts on this northerly flow gives rise to a westward acceleration, maintaining the AEJ. The mid-troposphere northerly flow over the Sahelian latitudes is missing in most of the state-of-the-art coupled models used for the fourth Assessment of IPCC (Cook and Vizy 2006). AM2.0, driven by the observed SST, can reasonably capture this mid-troposphere northerly, but with slightly weaker strength (Fig. 5b), in alignment with the less accentuated AEJ (Fig. 4b).

4 Reproduction of the historical Sahel rainfall

AM2.0 shows good skills in capturing the late twentieth century Sahel drought and the associated circulation fields. The blue line in Fig. 6 shows the ensemble mean JAS SRI simulated by GOGA experiment, with the ±1 standard deviation of the ensemble spread indicated by the shading. The correlation between GOGA simulation and the observed index (red, calculated based on the station records of accumulated monthly rainfall from the NOAA Global Historical Climate Network, GHCN, Easterling et al. 1996) during 1950–2000, is 0.6 and 0.3 for the detrended indices. Thus, the skill of the GOGA simulation mostly comes from the multidecadal time scale. At interannual time scales, it has been reported that ENSO can influence Sahel climate, with warm (cold) ENSO phase usually driving a drying (moistening) over Sahel (e.g., Nicholson and Kim 1997; Rowell 2001; Janicot et al. 2001). But the composite analysis of the Sahel rainfall with respect to Niño 3.4 SST index shows that AM2 tends to overreact to the cold phase of the ENSO, opposite to the observed preferential responsiveness of Sahel to the warm ENSO phase (Janicot et al. 2001).

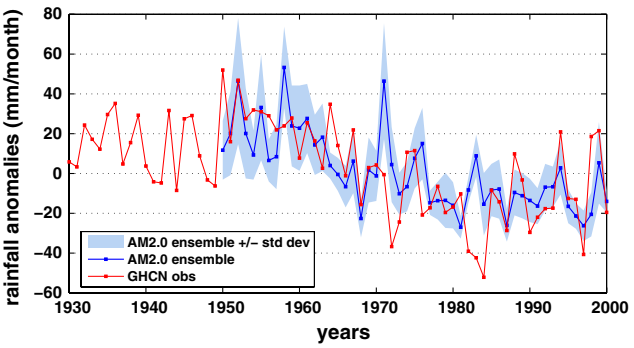

Fig. 6 The JAS SRI (in mm month^{-1}) from GHCN station data (*red*), simulated by AM2.0 GOGA (*blue*). The *light blue* shading represents the ±1 standard deviation within the ensemble of GOGA simulations. The anomalies are derived with respect to the mean over 1950–2000

To estimate the signal to noise ratio of Sahel rainfall in AM2, we adopt from Koster et al. (2000) the measure of the tightness of the ensemble spread, or coherence among realizations:

$$\Omega = \frac{I\sigma^2_{\text{Forced}} - \sigma^2_{\text{Total}}}{(I-1)\sigma^2_{\text{Total}}}$$

where I is ensemble size (10), σ^2_{Total} is the variance of the stacked time series of the 10 realizations, σ^2_{Forced} refers to the variance forced by the prescribed SST boundary conditions. In the limit of infinitely large ensemble size, the "Forced" component is asymptotic to variance of the ensemble mean time series, while the "internal" component of the variance that arises from land-atmosphere interaction, is represented by the difference of $\sigma^2_{\text{Total}} - \sigma^2_{\text{Forced}}$. Provided that the 10-member ensemble mean represents the SST-forced signal, we estimated σ^2_{Total} and σ^2_{Forced} to be 561 and 364 mm^2 day^{-2}, respectively, giving rise to an Ω of 0.61. This number represents a substantial amount of internal variability, somewhat larger compared to the coherence estimated for the Sahel rainfall variability (which is 0.7) in NSIPP1 (Giannini et al. 2005). Nevertheless, the ratio of the "forced" to the "internal" variance is still approximately 1.8, implying the dominance of SST boundary forcing for the Sahel rainfall variability in AM2.0.

Few if any of the individual realizations of AM2.0 captures the extreme dry episode between 1982 and 1984. Aside from the considerable intrinsic atmospheric variability demonstrated above, this could also be related to the deficiency of representing atmosphere-ocean interaction with SST-forced simulations (Tippett 2006), the missing feedback processes such as the dynamical vegetation (Zeng et al. 1999), dust aerosol (Yoshioka et al. 2007), and/or volcanic forcing due to the eruption of El Chichon in 1982.

All three classes of AM2.0 AMIP runs reproduce realistically the pattern of the linear trend of the African rainfall from 1950 through 2000 (Fig. 7). The inter-comparison among them seems to suggest the dominance of the tropical Indo-Pacific SST forcing (Fig. 7d) in the Sahel rainfall trend in AM2.0. This is somewhat at odds with the conventional notion that the interhemispheric SST dipole over the Atlantic plays substantial role in the low-frequency variability of the Sahel rainfall (e.g., Ward 1998; Folland et al. 1986, 1991; Rowell et al. 1995; Fontaine et al. 1998; Zhang and Delworth 2006; Hoerling et al. 2006). Great caution should be used in interpreting this result because it is clearly model-dependent. The stronger sensitivity of AM2.0 to the Indo-Pacific SST warming (relative to previous model studies) versus the Atlantic dipole, is likely one of the underlying reasons for the projection of a strong future drying trend over the Sahel under global warming by the GFDL coupled model CM2.0 (Held et al. 2005; Biasutti et al. 2008).

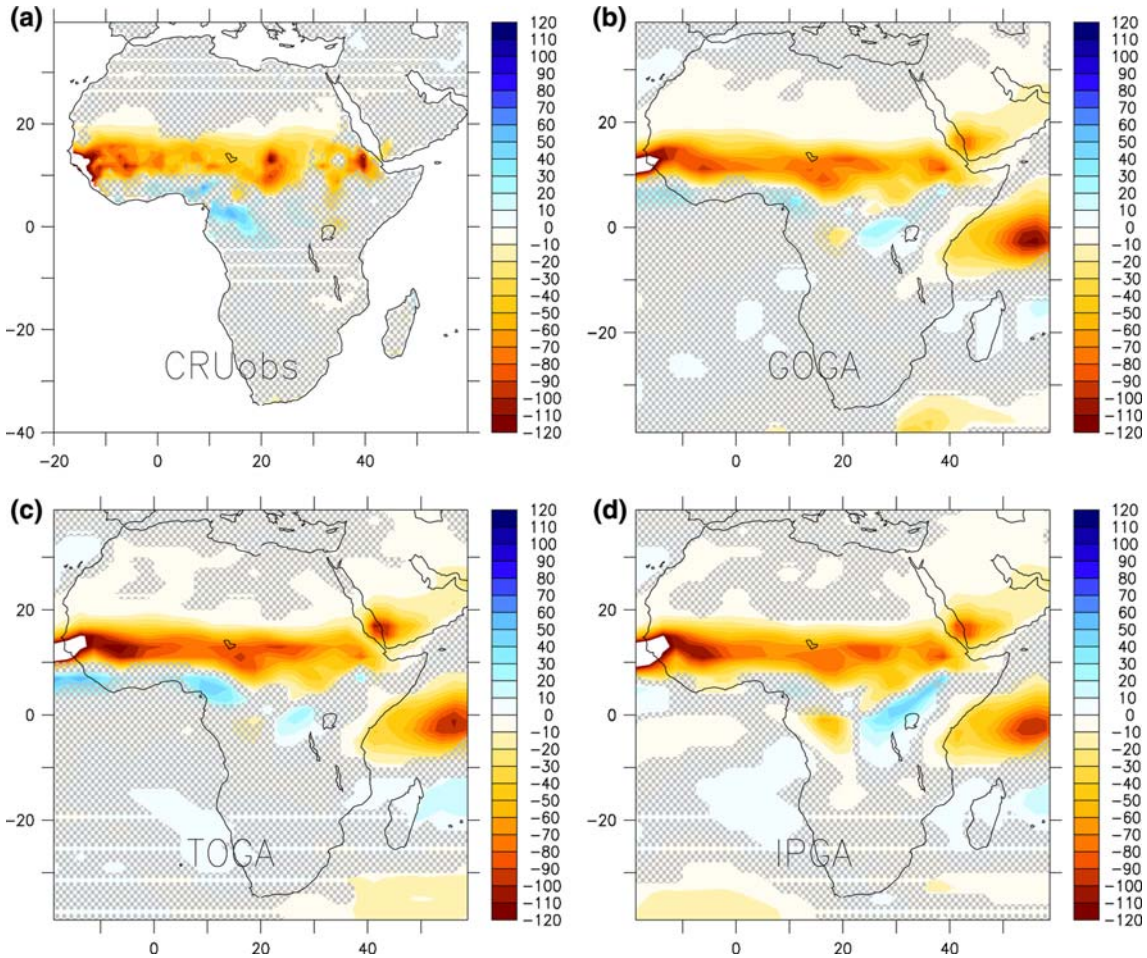

Fig. 7 The linear JAS precipitation trend from 1950 to 2000 (in mm month^{-1} 50 years^{-1}) calculated from CRU-TS_2.1 land precipitation data (**a**); AM2.0 ensemble mean precipitation of GOGA (**b**); TOGA (**c**); and IPGA (**d**). The hatched areas are not significantly different from zeros at 5% level based on Student's *t*-test

The insensitivity of AM2.0 to the Atlantic dipole forcing can also be readily discerned from the comparison of the trend in vertical velocity (omega) during 1958–1994 between the GOGA simulation and ECMWF reanalysis data (Fig. 8a, b). Over the Sahel region, the modeled omega field compares reasonably well with the reanalysis, even the dipole structure near the shallow convection region between 12°N and 25°N is captured. However, the strong ascent associated with intensified convection to the south of Sahel and descent to the south of the equator are both missing in the GOGA simulation. As such, while the trend of the reanalysis consists of a component of southward shift, the modeled trend is characteristic of an overall weakening of the tropical African rainbelt. At this point, we are not clear if this discrepancy is due to the deficiency of AM2.0 or the quality of the ECMWF reanalysis, since it still remains an issue of debate as to the relative importance of the southward shift and the overall weakening of the rainbelt in the Sahel drought from the precipitation data (e.g., Shinoda and Kawamura 1994).

Overall, AM2.0 reproduces the hallmarks for the Sahel drying trend—southward shift in AEJ and the weakening of TEJ (Fig. 8c, d). Particularly, the alignment of the dipolar zonal wind anomalies with the background mean winds in the mid-troposphere indicates reduced zonal wind shear and barotropic instability on the cyclonic side of the AEJ and reduced vertical wind shear and baroclinic instability on the anti-cyclonic side of the AEJ. Both are argued to be important source of energy conversion for African Easterly wave development (e.g., Reed et al. 1988; Thorncroft and Hoskins 1994).

5 The mechanisms of the Indian Ocean SST forcing

5.1 Sahel rainfall and moisture transport

We now focus our attention on the role of the Indian Ocean warming in drying the Sahel. The SST pattern used to drive the IND MS experiment (Fig. 9, area within the box) is

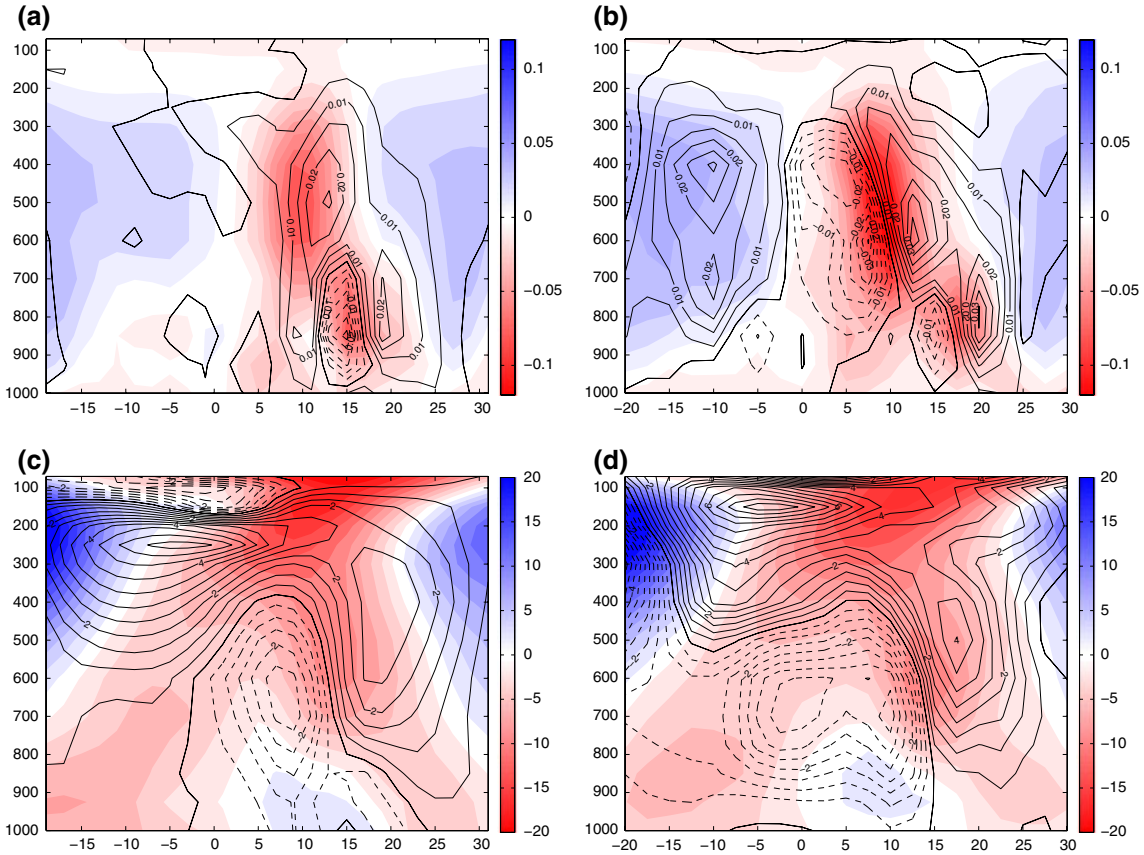

Fig. 8 Comparison of summer circulation trend between the GOGA simulations and the ECMWF reanalysis. Top (bottom) panels are the linear trend during 1958 to 1994 in vertical pressure velocityω (zonal wind) averaged between 20°W and 40°E. *Left* (*right*) panels are for the AM2.0 GOGA simulation (ECMWF reanalysis). The background shadings are the corresponding climatological fields. Note the *red* denotes negative values. Contour interval for zonal wind (vertical pressure velocity) is 0.5 m s^{-1} (0.005 Pa s^{-1})

derived by regressing the 5-year low pass global SST against the same filtered SRI during 1901–2002. The hatched areas are where the correlation between the local SST and SRI is not significantly different from zero with 95% confidence based on the Student's *t*-test, in which the reduction of effective degrees of freedom due to serial correlation has been taken into account (von Storch and Zwiers 1999). In addition to the equatorial and southern subtropical Indian Ocean and south Atlantic, there are high and significant loadings over the mid and high latitudes over the North Pacific and North Atlantic oceans.

The precipitation response to the Indian Ocean SST warming includes increase over the tropical Indian Ocean, the Indian subcontinent and Southeast Asia, and decrease over the most of the tropical African rainbelt (Fig. 10a). The precipitation is consistent with the divergence/convergence of the total moisture flux (Fig. 10b). Comparing the convergence of moisture flux between that caused by the change of specific humidity (Fig. 10c) and that by the change of winds (Fig. 10d) over the north Indian Ocean, we notice that the latter appears to be an amplification of the former. We conjecture that the response over the Indian Ocean is initiated by the enhanced moisture convergence due to the increased humidity (i.e., $\langle q' \bar{\mathbf{v}} \rangle$, Fig. 10c), and that the wind response to the original convection anomalies reinforces the original moisture convergence and intensifies the precipitation response. Over the tropical Africa, the anomalous moisture flux is whereas predominantly controlled by the change of winds (i.e., $\langle \bar{q}\, \mathbf{v}' \rangle$, Fig. 10d). The eastward moisture fluxes that feed into the intensified convection over the Indian Ocean are a likely to play a significant role in the moisture deficit of the Sahel. The same pattern of moisture flux has been also found in similar experiments with several different models forced by a warming over the Indian Ocean (Shuanglin Li 2008, personal communication). The low-level equatorial westerly along with cyclonic gyre circulation at its off-equator flanks, can be largely interpreted as the Gill-like (Gill 1980) response to the intensified convective heating over the Indian Ocean.

5.2 Response in circulation

Examining the rotational component of the wind fields reveals the important role of the equatorial wave dynamics

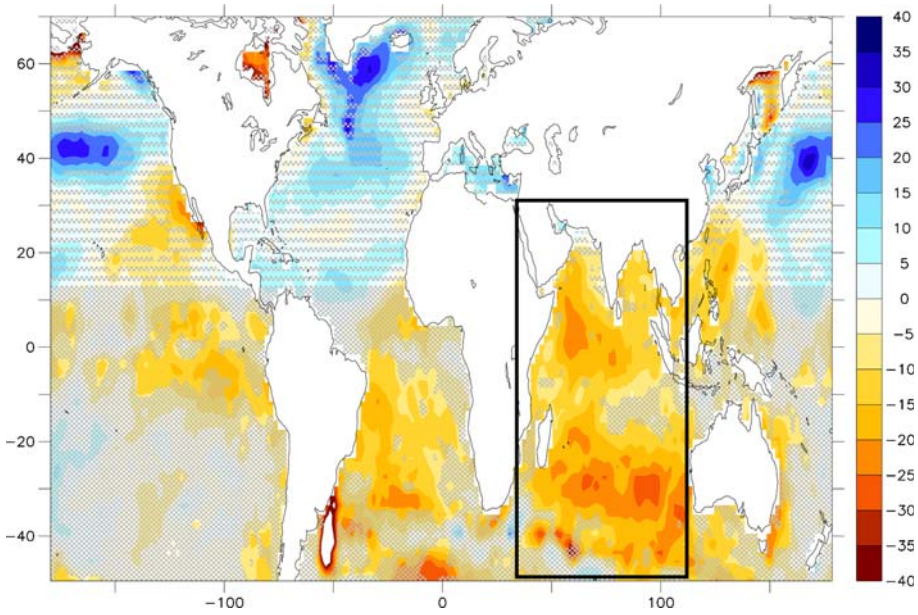

Fig. 9 Regression pattern of JAS SSTs against the observed SRI during 1903–2000. Both SSTs and SRI have been filtered by 5-year running mean prior to the regression. The hatched areas are where the regression coefficients are not significantly different from zero based on Student's *t*-test with the reduction of degrees of freedom due to serial correlation considered. Unit is 10^{-2} K std^{-1} of SRI

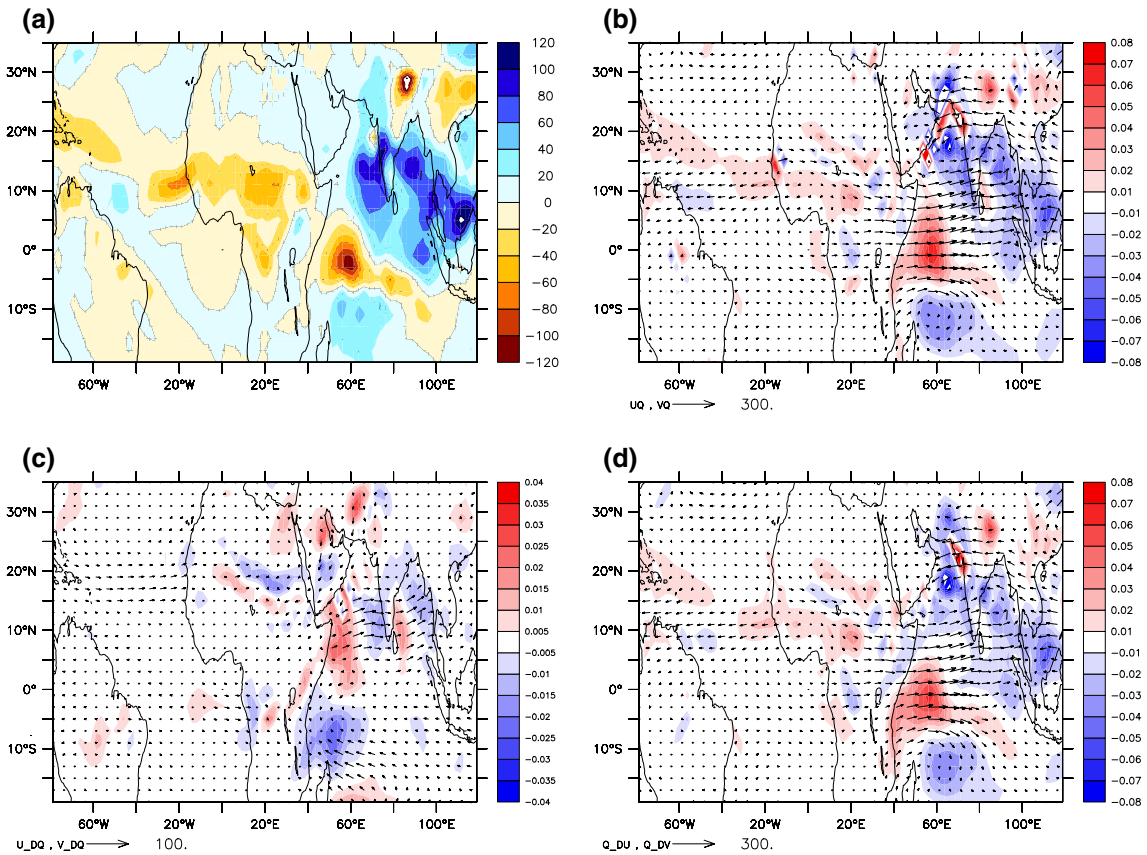

Fig. 10 Responses to the Indian Ocean SST anomalies in Expt. IND MS. (**a**) precipitation (mm day^{-1}); (**b**) vertically integrated moisture flux (*arrows*, in unit of Kg m^{-1} s^{-1}) and its divergence (*shading*, in unit of g m^{-2} s^{-1}); (**c**) anomalous moisture flux due to changes in specific humidity ($\langle q'\bar{\mathbf{v}}\rangle$) and the associated divergence; (**d**) similar to (**c**) but for the anomalous flux and divergence due to the change in winds ($\langle \bar{q}\mathbf{v}'\rangle$)

in the response to the Indian Ocean warming. Figure 11a, b delineates the lower (upper) level eddy streamfunction and divergence wind field at 700 hPa (200 hPa). The strong low-level convergence and upper-level divergence over the Indian Ocean, as indicated by the arrows of divergent wind component, represent the intensified deep convection and

mid-tropospheric ascent. The anti-symmetry between the rotational winds in the upper tropical troposphere (200 hPa) and the lower troposphere (700 hPa) over the Africa-Indian Ocean sector can be readily interpreted as a Gill-type atmospheric response (Gill 1980; Heckley and Gill 1984) to the convective heating over the Indian Ocean (centered at 70°E). According to this theory, equatorial heating can drive descent off the equator near the Rossby wave front to the west of the heating. The descending motion over the North Africa is connected dynamically to the Indian Ocean heating in a similar way. As will be shown later in a transient adjustment to a sudden switch-on of Indian Ocean forcing, it is the equatorial Rossby wave propagation that communicates the warming signal from the Indian Ocean to Africa and suppresses convection there. The resultant equilibrium response may be viewed as well as an anomalous Walker circulation with a rising branch over the Indian Ocean and descending branch over the Africa, as depicted in the height-longitude cross section of zonal wind and pressure velocity fields (averaged between equator and 15°N, Fig. 11c).

5.3 Moist processes in the time-dependent response

To further demonstrate the relevance of the Gill-type solution in moist dynamics to the simulated Sahel drought, a large ensemble (40-member) experiment is carried out by suddenly introducing the same SST warming as in Exp. IND MS from June 1st but with an amplified magnitude (corresponding to four times of the standard deviation of the low pass filtered SRI). The large ensemble and forcing amplitude allow us to filter out the noise and examine the transient dynamical processes and their interaction with the moist processes during the initial phase of the adjustment.

To demonstrate the role of the wave dynamics in the adjustment to the sudden swith-on of the Indian Ocean SST warming, we show (Fig. 12) the tropospheric mean temperature averaged over 200–850 hPa and between 20°S and 20°N for the Africa-Indo-Pacific longitudes from Day 1–20. During the first 2 weeks or so, the propagating features of Kelvin waves and Rossby waves can be readily recognized. The Kelvin wavefront propagates at a phase speed of $\sim$12 m s^{-1}, three times as fast as the phase speed of the westward propagating Rossby wave front ($\sim$4 m s^{-1}), consistent with that predicted by the moist equatorial wave theory (Neelin and Yu 1994; Emaneul et al. 1994). These phase speeds are much slower than their corresponding dry equatorial waves of the first baroclinic mode (Rodwell and Hoskins 1996). The Rossby wave front picks up speed once it reaches the African continent, consistent with the increase in the effective moist static stability, due to the small specific humidity over the African continent.

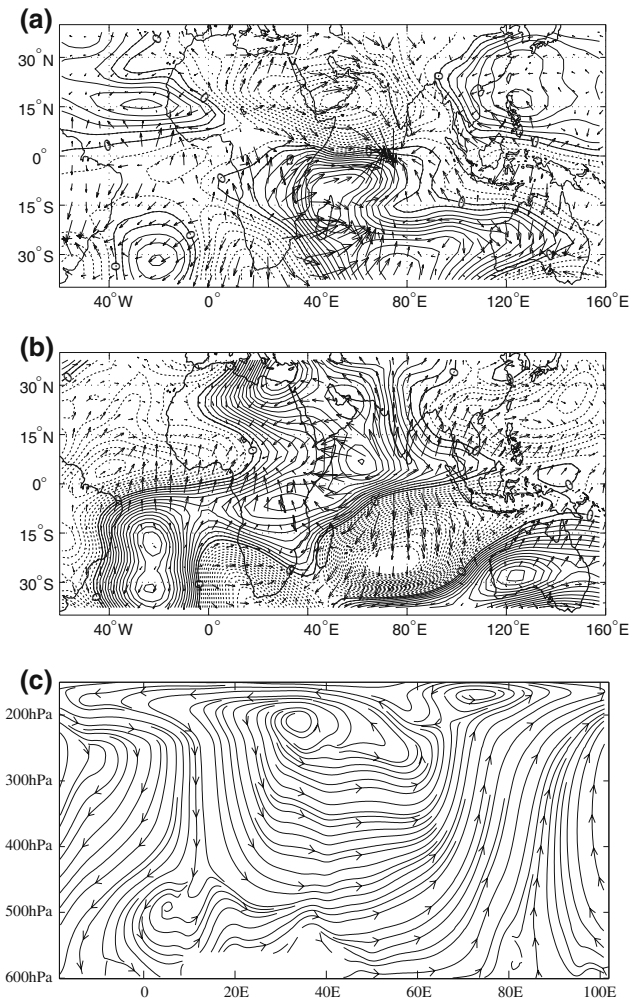

Fig. 11 The circulation response to Indian ocean SST anomalies in Expt. IND-MS. (**a**) 700 hPa eddy streamfunction (contours) and divergent wind (*arrows*); (**b**) 200 hPa eddy streamfunction (contours) and divergent wind (*arrows*); (**c**) longitude-height cross-section of the streamlines for u and $-\omega$ fields averaged between equator and 15°N. The vertical scale of ω is arbitrary

Upon the arrival of the warming signal, the air column over the Sahel shows some interesting feedbacks involving moist processes. Figure 13 presents the temporal evolution of the vertically integrated tropospheric temperature (square), specific humidity (open circle) and precipitation (filled circle) averaged over the Sahel. During the first 2 weeks or so, precipitation and specific humidity (temperature) undergo monotonic decrease (increase). The total cloud amount and the associated longwave radiative forcing decrease as well (not shown). During the initial phase of the adjustment, the vertical profile of the tropospheric temperature is characterized by a warmer temperature aloft than below, indicative of increased static stability. Therefore, the rising temperature during the initial phase also represents the stabilizing trend of the Sahelian air column, and is initially driven by adiabatic subsidence. Additionally, the

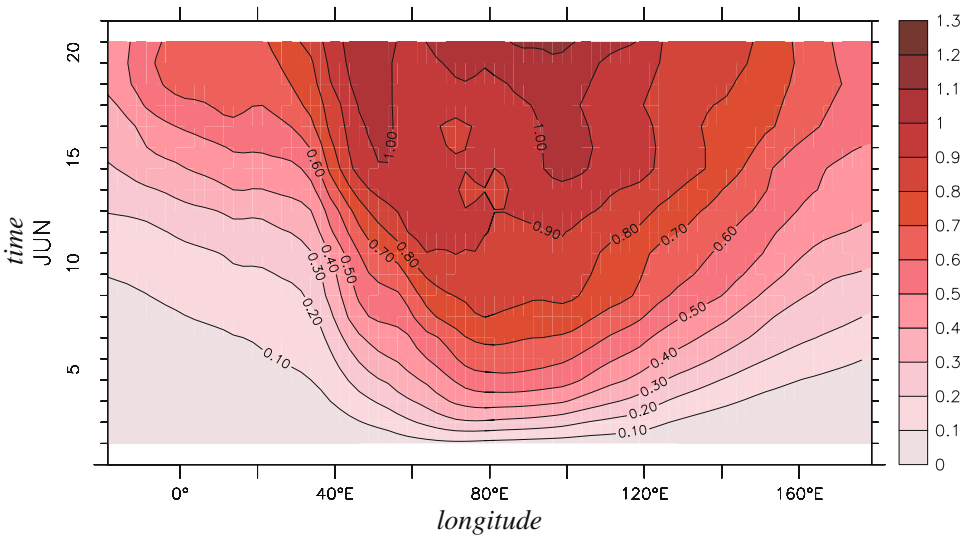

Fig. 12 Hovmoller diagram, in time-longitude space, of the tropical mean (20°S–20°N) tropospheric mean (200–850 hPa) temperature response to the switch-on of Indian Ocean forcing from June 1st. The unit is °K

subsidence at the Rossby wave front expels the low-level moisture out of the Sahel region causing a moisture deficit. The larger stratification and lower humidity work in tandem to impede the formation of convective precipitation. The associated lack of condensational heating would cause cooling to the air column, therefore the rising temperature during the initial adjustment is not diabatically driven, but originates from the dynamically-induced subsidence.

Meanwhile, the cooling associated with the reduced convection and condensation (Fig. 14, orange shading) and reduced long wave radiative forcing (Fig. 14, red shading) in turn reinforce the dynamically induced subsidence. Without this diabatic feedback, the adiabatic descent can only glide along isentropic surfaces, and could not produce such a strong subsidence as simulated by the full moist model. We have conducted experiments using a linearized dry dynamics primitive equation model (Held and Suarez 1994) with different choices of model parameters and background states, and none produces as a strong subsidence as simulated by the AM2.0. Studies using a dry dynamical model with similar configurations (Rodwell and Hoskins 1996) point to a similar conclusion that the remote, equatorially confined, diabatic heating can not induce significant localized descent. The important role of this "precipitation feedback" has also been explicitly identified by Lintner and Chiang (2006), who examined the adjustment of the remote tropics to a rapid onset of a SST warming over the equatorial eastern Pacific and compared the cases with and without the feedback of moist convection.

In summary, these transient adjustment processes suggest that the initial phase of response is governed by the equatorial wave dynamics, while the diabatic processes serve as important feedbacks to the dynamically initiated signal. It is of interest to note that the diabatic feedbacks are naturally more prominent over the regions where tropical convection already exists in the climatological state.

At the end of the initial linear adjustment, the system starts to rebound toward, but never returns to the neutral condition. After 3 weeks or so, the system enters the equilibrating phase and all variables start to fluctuate irregularly around an equilibrium state. The equilibrium state of Sahel seems to be consistent with another aspect of the wave dynamics: the near surface westerly wind, which itself is a dynamical response to the convective heating

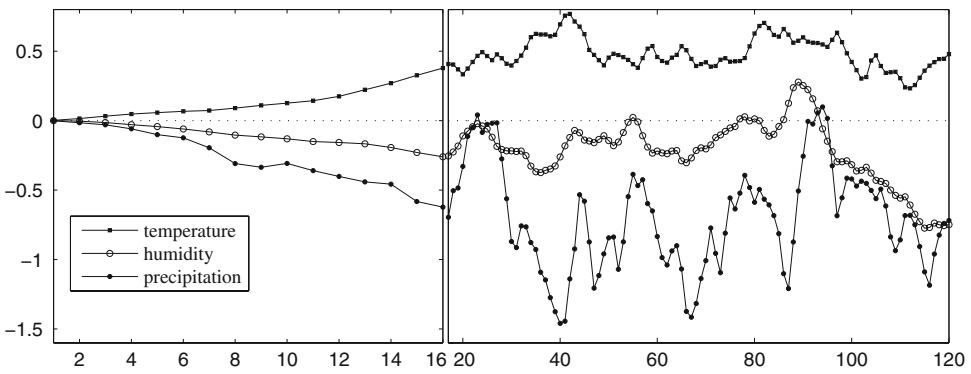

Fig. 13 The transient response of vertically integrated temperature (*square*, in °K), specific humidity (*open circle*, in kg kg^{-1}) between surface and 300 hPa and precipitation (*filled circle*, in mm day^{-1}) to the switch-on of Indian SST forcing. The initial 25 days are stretched to illustrate the initial phase of the adjustment

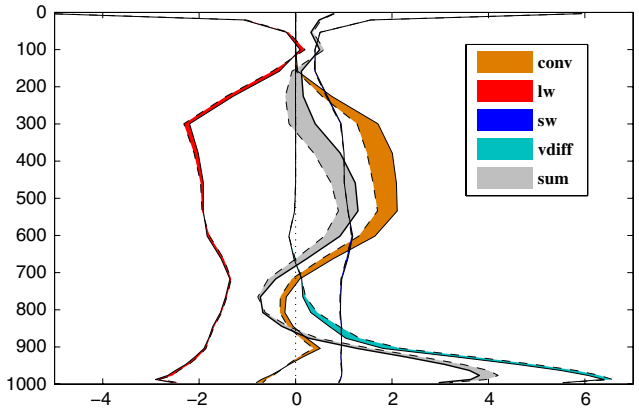

Fig. 14 JAS seasonal mean vertical diabatic heating profiles averaged over the Sahel region (10°W–40°E, 10–20°N). The solid lines are for the heating terms in the control experiment, and the dashed lines for the IND SST perturbation experiment. The departure of the perturbation experiment from the control for different terms is depicted by color shading. The unit is K day^{-1}

from the Indian Ocean, drawing moisture out of the African continent and into the ocean, desiccating the land. The availability of moisture is the most critical factor for sustaining the original convection at the face of free atmosphere warming (Neelin et al. 2003; Chou and Neelin 2004; Neelin and Su 2005). Therefore, under the influences of both the atmospheric stabilization from above and moisture deprivation from below, Sahel ultimately respond with a suppressed precipitation to the Indian Ocean warming.

In alignment with the reduced convection, the vertical diabatic heating profile (Fig. 14) is characteristic of cooling in the free troposphere and heating below 800 hPa (see the gray shading), the former due in large degree to the anomalous latent heat release (orange shading) and long wave radiative cooling (red shading), the latter to the near surface sensible heat flux. This heating profile tends to compensate for the adiabatic warming and stabilization and restore the thermal structure back towards the moist adiabat. While the radiatic forcing associated with the adjustment in stratus clouds and short wave radiation only play minor roles in this experiment.

6 Summary and discussion

Suites of experiments have been conducted with GFDL's AM2.0 atmospheric general circulation model to examine the role of the Indian Ocean warming in the late twentieth century Sahel drought, and to assess the fidelity of this model in reproducing the tropical circulation and precipitation climate over the Atlantic-Africa sector, as well as the observed history of the Sahel rainfall index. The results are summarized as follows:

- The AM2.0, forced by the observed SST boundary condition, can realistically simulate the three-dimensional structure of the climatologically mean circulation over the tropical Africa. AM2.0 also produces realistic distribution of the mean rainfall and its annual cycle, and simulates reasonably the spatial distribution of the variability of the summer rainfall over the Atlantic-Africa sector. In addition, the model can faithfully capture the spatial characteristics of the leading modes of rainfall variability (EOF) of the tropical African rainfall.
- When forced with the observed history of the SSTs, the AM2.0 is capable of reproducing the spatial pattern and amplitude of the observed Sahelian drying in the late twentieth century. The associated circulation can also be reasonably captured by the AM2.0.
- The mechanisms of the Indian SST forcing have been the focal point of this study. In the AM2.0, a warmer Indian Ocean enhances the local convection, the associated latent heat release warms up and stabilizes the surrounding tropical troposphere through the propagation of equatorial waves. To the west of the heating source, the equatorial Rossby wave front, which carries mid-tropospheric descent and warming with it, sets off a chain of feedbacks to suppress convection over tropical Africa. These feedbacks include the depletion of moisture by the low-level divergence, the amplification of the original subsidence by the mid-tropospheric cooling associated with the muted convection, and the net cloud radiative cooling associated with the less deep cumulus clouds. The equilibrated state of the Sahelian precipitation is controlled not only by the dynamically induced warming and column stabilization, but also by the reduced availability of moisture. The latter, in large degree, can be ascribed to the low-level equatorial westerly, which itself is a part of the gravest Rossby wave response to the convective heating over the Indian Ocean.

In this study, we have extensively employed AMIP-type prescribed-SST experiments to probe the mechanisms of Sahel drought. However, prescribing SST poses a risk of distorting the dynamics of the actually coupled system (Tippett 2006), especially in the Indian Ocean-Asian Monsoon area (Douville 2005; Copsey et al. 2006; Wang et al. 2005). The association between the warming SST and the above-average precipitation in the AMIP framework often breaks down when the ocean is free to interact with the atmosphere. For example, at interannual time scales, the warm SSTs in the Indian Ocean during the boreal summer, rather than causing an increase of precipitation, are usually the result of reduced deep convection and cloud cover, and the consequent increase of incoming solar

radiation at the surface (Rao and Goswami 1988; Kirtman and Shukla 2002). The approach of prescribing Indian Ocean SST warming in the AMIP experiments can only be valid to the extent that the warming is externally forced, say, from the radiative effects of increased greenhouse gas concentration, or from the ocean heat fluxes induced by the ocean circulation. Studies indeed suggest that the secular warming trend of the Indian Ocean during the twentieth century is in large degree attributable to increasing greenhouse gas forcing (Knutson et al. 1999, 2006; Hurrell et al. 2004), and the warming concurs with the increase of convective clouds and decrease of short wave radiation (Du and Xie 2008). Nevertheless, the limitations inherent in the prescribed-SST simulations need to be kept in mind.

Even though the Indian Ocean warming can be construed to be GHG driven, and may have contributed to the drying of Sahel during the late twentieth century, one should not conclude hastily that the Sahel will become drier as Indian Ocean continues to warm. For one reason, the link between Indian Ocean warming and above-average rainfall may be much less strong in a coupled system; for another, the tropical atmospheric stratification is set by the maximum convection, which, in a warmed climate, may not occur over Indian Ocean. In an analysis (Vecchi and Soden 2007, see their Fig. 7) of the simulations for the A1B climate change scenario for the Fourth Assessment of the IPCC report, the maximum increase of convection occurs near the central equatorial Pacific, whereas, there is a weakening of the upward motion over the Indian Ocean. Strictly speaking, in this warming scenario, it is the "El Nino-like" equatorial central Pacific warming, instead of the Indian Ocean, plays the role of stabilization as the Indian Ocean warming in our IND-MS experiment, while the effect of Rossby wave-induced moisture flux, if any, may not reach African continent at all.

The rendition of Sahel response would still be drying if the stabilization mechanism acted in isolation, no matter from Indian Ocean or central Pacific. However, the prospect of Sahelian climate as response to GHG warming is further complicated by other factors such as (i) the SST changes over other world oceans, especially the differential warming of the North Atlantic versus the South Atlantic (Hoerling et al. 2006); and (ii) the direct radiative effect of GHG forcing, which, acting in isolation, can warm the land preferentially relatively to the ocean and drive a monsoon-like onshore circulation, and hence to enhance the rainfall over the land. The future prospect of the Sahelian climate depends not only on the sensitivity to the same SST pattern and/or GHG forcing, but also on how the SST responds to GHG forcing as an interactive factor of coupled climate system. The uncertainties in the future Sahelian climate will persist until the climate models can accurately handle the intricacy of these sensitivities.

Acknowledgements I like to first acknowledge Drs. I. M. Held and T. L. Delworth for their mentorship during my visit at GFDL when the reported work was carried out. I am indebted to A. Giannini and M. Biasutti for providing the station based Sahel rainfall index and data from the NSSIP1 simulations and their helpful comments during the formative stage of the paper. I would like to express my appreciation to M. Hoerling and another anonymous reviewer for their perceptive review, which helps improve substantially the manuscript. I also thank G. Meehl and A. Sealy for their encouragement and conducting the NCAR internal review. I acknowledge the Climate Research Unit at University of East Anglia for providing the gridded land precipitation data set. X. Jiang provided the linearized dry GCM for the experiments on the dry response to a prescribed equatorial heating. J. Lu is supported by the Advance Study Program (ASP) at NCAR.

References

Bader J, Latif M (2003) The impact of decadal-scale Indian Ocean sea surface temperature anomalies on Sahelian rainfall and the North Atlantic Oscillation. Geophys Res Lett 30(22):2169. doi:10.1029/2003GL018426

Biasutti MB, Held IM, Sobel AH, Giannini A (2008) SST forcings and Sahel rainfall variability in simulations of the 20th and 21st centuries. J Clim 21:3471–3486. doi:10.1175/2007JCL11896.1

Chou C, Neelin JD (2004) Mechanisms of global warming impacts on regional tropical precipitation. J Clim 17:2688–2701. doi:10.1175/1520-0442(2004)017<2688:MOGWIO>2.0.CO;2

Cook KH, Vizy EK (2006) Coupled model simulations of the West African Monsoon system: 20th and 21st century simulations. J Clim 19:3681–3703. doi:10.1175/JCLI3814.1

Copsey D, Sutton R, Knight JR (2006) Recent trends in sea level pressure in the Indian Ocean region. Geophys Res Lett 33:L19712. doi:10.1029/2006GL027175

Delworth TL et al (2006) GFDL's CM2 global coupled climate models. Part I: formulation and simulation characteristics. J Clim 19:643–674. doi:10.1175/JCLI3629.1

Douville H (2005) Limitations of time-slice experiments for predicting regional climate change over South Asia. Clim Dyn 24:373–391. doi:10.1007/s00382-004-0509-7

Du Y, Xie S-P (2008) Role of atmospheric adjustments in the tropical Indian Ocean warming during the 20th century in climate models. Geophys Res Lett 35:L08712. doi:10.1029/2008GL033631

Easterling DR, Peterson TC, Karl TR (1996) On the development and use of homogenized climate data sets. J Clim 9:1429–1434. doi:10.1175/1520-0442(1996)009<1429:OTDAUO>2.0.CO;2

Emaneul KA, Neelin DJ, Bretherton CS (1994) On large-scale circulations in convecting atmospheres. Q J R Meteorol Soc 120:1111–1143. doi:10.1002/qj.49712051902

Folland CK, Palmer TN, Parker DE (1986) Sahel rainfall variability and worldwide sea temperature, 1901–85. Nature 320:602–606. doi:10.1038/320602a0

Folland CK, Owen J, Ward MN, Colman A (1991) Prediction of seasonal rainfall in the Sahel region using empirical and dynamical methods. J Forecast 10:21–56. doi:10.1002/for.3980100104

Fontaine B, Trzaska S, Janicot S (1998) Evolution of the relationship between near global and Atlantic SST modes and the rainy season in West Africa: statistical analyses and sensitivity experiments. Clim Dyn 14:353–368. doi:10.1007/s003820050228

GFDL's GAMDT Global Atmospheric Model Development (2004) The new GFDL global atmospheric and land model AM2/LM2: evaluation with prescribed SST simulations. J Clim 17:4641–4673. doi:10.1175/JCLI-3223.1

Giannini A, Saravanan R, Chang P (2003) Oceanic forcing of Sahel rainfall on interannual and to interdecadal time scales. Science 302:1027–1030. doi:10.1126/science.1089357

Giannini A, Saravanan R, Chang P (2005) Dynamics of the boreal summer African monsoon in the NSIPP1 atmospheric model. Clim Dyn 25:517–535. doi:10.1007/s00382-005-0056-x

Giannini A, Biasutti M, Held IM, Sobel AH (2008) A global perspective on Afircan climate. Climatic Change 90:359–383. doi:10.1007/s10584-008-9396-y

Gill AE (1980) Some simple solutions for heat-induced tropical circulation. Q J R Meteorol Soc 106:447–462. doi:10.1002/qj.49710644905

Gleckler PJ, Taylor KE, Doutriauz C (2008) Performance metrics for climate models. J Geophys Res 113:D06104. doi:10.1029/2007JD008972

Grist JP, Nicholson SE (2001) A study of dynamics factors influencing the rainfall variability in the west African Sahel. J Clim 14:1337–1359. doi:10.1175/1520-0442(2001)014<1337:ASOTDF>2.0.CO;2

Hagos SM, Cook KH (2008) Ocean warming and the late-twentieth-century Sahel drought and recovery. J Clim 21:3797–3814. doi:10.1175/2008JCLI2055.1

Hastenrath S (1990) Decadal-scale changes of the circulation in the tropical Atlantic sector associated with Sahel drought. Int J Climatol 10:459–472. doi:10.1002/joc.3370100504

Hastenrath S, Wolter K (1992) Large-scale patterns and long term trends of circulatioin variability associated with Sahel rainfall anomalies. J Meteorol Soc Jpn 70:1045–1055

Heckley WA, Gill AE (1984) Some simple analytical solutions to the problem of forced equatorial long waves. Q J R Meteorol Soc 110:203–217. doi:10.1002/qj.49711046314

Held IM, Suarez MJ (1994) A proposal for the intercomparison of the dynamical cores of atmospheric general circulation models. Bull Am Meteorol Soc 75(10):1825–1830. doi:10.1175/1520-0477(1994)075<1825:APFTIO>2.0.CO;2

Held IM, Delworth TL, Lu J, Knutson T, Findell K (2005) Simulations of Sahel drought in the 20th and 21st centuries. Proc Natl Acad Sci USA 102(50):17891–17896. doi:10.1073/pnas.0509057102

Hoerling MP, Hurrell JW, Eischeid J, Phillips AS (2006) Detection and attribution of 20th century Northern and Southern African monsoon change. J Clim 19:3989–4008. doi:10.1175/JCLI3842.1

Hurrell JW, Hoerling MP, Phillips AS, Xu T (2004) Twentieth century north Atlantic climate change. Part I: assessing determinism. Clim Dyn 23:371–389. doi:10.1007/s00382-004-0432-y

Janicot S, Moron V, Fontaine B (1996) Sahel drought and ENSO dynamics. Geophys Res Lett 23(5):515–518. doi:10.1029/96GL00246

Janicot S, Trzaska S, Poccard I (2001) Summer Sahel-ENSO teleconnection and decadal time scale SST variations. Clim Dyn 18:303–320. doi:10.1007/s003820100172

Kang SM, Held IM, Frierson DWM, Zhao M (2008) The response of the ITCZ to extratropical thermal forcing: Idealized slab-ocean experiments with a GCM. J Clim 21:3521–3532. doi:10.1175/2007JCLI2146.1

Kirtman BP, Shukla J (2002) Interactive coupled ensemble: a new coupling strategy for CGCMs. Geophys Res Lett 29(10). doi:10.1029/2002GL014834

Knutson TR, Delworth TL, Dixon KW, Stouffer RJ (1999) Model assessment of regional surface temperature trends (1949–1997). J Geophys Res 104(24):30981–30996. doi:10.1029/1999JD900965

Knutson TR, Delworth TL, Dixon KW, Held IM, Lu J, Ramaswamy V, Schwarzkopf MD, Stenchikov G, Stouffer RJ (2006) Assessment of twenty-century regional surface temperature trends using the GFDL CM2 coupled models. J Clim 19:1624–1651. doi:10.1175/JCLI3709.1

Koster RD, Suarez MJ, Heiser M (2000) Variance and predictability of precipitation at seasonal-to-interannual timescales. J Hydrometeorol 1:26–46. doi:10.1175/1525-7541(2000)001<0026:VAPOPA>2.0.CO;2

Lamb PJ (1978) Case studies of tropical Atlantic surface circulation patterns during recent sub-Saharan weather anomalies: 1967 and 1968. Mon Wea Rev 106:482–491

Levitus S, Antonov JI, Boyer TP, Stephens C (2000) Warming of global ocean. Science 287:2225–2229. doi:10.1126/science.287.5461.2225

Lintner BR, Chiang JCH (2006) Adjustment of the remote tropical climate system to El Nino conditions. J Clim 20:2544–2557. doi:10.1175/JCLI4138.1

Lu J, Delworth TL (2005) Oceanic forcing of the late 20th century Sahel drought. Geophys Res Lett 32:22706. doi:10.1029/2005GL023316

Milly PCD, Shmakin AB (2002) Global modeling of land water and energy balances. Part I: the land dynamics (LaD) model. J Hydrometeorol 3:283–299. doi:10.1175/1525-7541(2002)003<0283:GMOLWA>2.0.CO;2

Mitchell TD, Jones PD (2005) An improved method of constructing a database of monthly climate observations and associated high-resolution grids. Int J Climatol 25:693–712. doi:10.1002/joc.1181

Neelin JD, Su H (2005) Moist teleconnection mechanisms for the tropical South American and Atlantic sector. J Clim 18:3928–3950. doi:10.1175/JCLI3517.1

Neelin JD, Yu J (1994) Modes of tropical variability under convective adjustment and the Madden-Julian oscillation. Part I: analytical results. J Atmos Sci 51:1876–1894. doi:10.1175/1520-0469(1994)051<1876:MOTVUC>2.0.CO;2

Neelin JD, Chou C, Su H (2003) Tropical drought regions in global warming and El Nino teleconnections. Geophys Res Lett 30:2275. doi:10.1029/2003GL018625

Nicholson SE, Grist JP (2001) A conceptual model for understanding rainfall variability in the West African Sahel on interannual and interdecadal timescales. Int J Climatol 21:1733–1757. doi:10.1002/joc.648

Nicholson SE, Kim J (1997) The relationship of the El Nino-Southern Oscillation to African rainfall. Int J Climatol 17:117–135. doi:10.1002/(SICI)1097-0088(199702)17:2<117::AID-JOC84>3.0.CO;2-O

Nicholson SE, Palao IM (1993) A re-evaluation of rainfall variability in the Sahel. Part I: characteristics of rainfall fluctuations. Int J Climatol 13:371–389. doi:10.1002/joc.3370130403

Palmer TN (1986) Influence of the Atlantic, Pacific and Indian Oceans on Sahel rainfall. Nature 320:251–253. doi:10.1038/322251a0

Rao KG, Goswami BN (1988) Interannual variations of sea surface temperature over the Arabian Sea and Indian monsoon: a new perspective. Mon Weather Rev 116(3):558–568. doi:10.1175/1520-0493(1988)116<0558:IVOSST>2.0.CO;2

Rayner NA, Parker DE, Horton EB, Folland CK, Alexander LV, Rowell DP, Kent EC, Kaplan A (2003) Global analyses of SST, sea ice, and night marine air temperature since the late nineteenth century. J Geophys Res 108(D14):4407. doi:10.1029/2002JD002670

Reed R, Hollingsworth A, Heckley W, Delsol F (1988) An evaluation of the performance of the ECMWF operational system in analyzing and forecasting easterly wave disturbances over Africa and tropical Atlantic. Mon Weather Rev 116:824–865. doi:10.1175/1520-0493(1988)116<0824:AEOTPO>2.0.CO;2

Rodwell MJ, Hoskins BJ (1996) Monsoons and the dynamics of deserts. Q J R Meteorol Soc 122:1385–1404. doi:10.1002/qj.49712253408

Rotstayn L, Lohmann U (2002) Tropical rainfall trends and the indirect aerosol effect. J Climate 15:2103–2116

Rowell DP (2001) Teleconnection between the tropical Pacific and the Sahel. Q J R Meteorol Soc 127:1683–1706. doi:10.1002/qj.49712757512

Rowell DP (2003) The impact of Mediterranean SSTs on the Sahelian rainfall season. J Clim 16:849–862. doi:10.1175/1520-0442(2003)016<0849:TIOMSO>2.0.CO;2

Rowell DP, Folland CK, Maskell K, Ward MN (1995) Variability of summer rainfall over tropical north Africa (1906–92): Observations and modeling. Q J R Meteorol Soc 121:669–704

Shinoda M, Kawamura R (1994) Tropical rainbelt, circulation, and sea surface temperatures associated with the Sahelian rainfall trend. J Metab Soc Jpn 72:341–357

Thorncroft CD, Hoskins BJ (1994) An idealized study of African easterly waves. I: a linear view. Q J R Meteorol Soc 120:953–982. doi:10.1002/qj.49712051809

Tippett MK (2006) Filtering of GCM simulated Sahel precipitation. Geophys Res Lett 33:01804. doi:10.1029/2005GL024923

Vecchi GA, Soden BJ (2007) Global warming and the weakening of the tropical circulation. J Clim 20:4316–4340. doi:10.1175/JCLI4258.1

Vizy EK, Cook KH (2001) Mechanisms by which Gulf of Guinea and eastern North Atlantic Sea surface temperature anomalies can influence African rainfall. J Clim 14:795–821. doi:10.1175/1520-0442(2001)014<0795:MBWGOG>2.0.CO;2

Vizy EK, Cook KH (2002) Development and application of a mesoscale climate model for the tropics: influence of sea surface temperature anomalies on the West African monsoon. J Geophys Res 107(D3):4023. doi:10.1029/2001JD000686

von Storch H, Zwiers FW (1999) Statistical analysis in climate research. Cambridge University Press, p 484

Wang B, Ding Q, Fu X, I-S K, Jin K, Shukla J, Doblas-Reyes F (2005) Fundamental challenge in simulation and prediction of summer monsoon rainfall. Geophys Res Lett 32:15711. doi:10.1029/2005GL022734

Ward MN (1998) Diagnosis and short-lead time prediction of summer rainfall in tropical North Africa at interannual and interdecadal timescales. J Clim 11:3167–3191. doi:10.1175/1520-0442(1998)011<3167:DASLTP>2.0.CO;2

Xie P, Arkin PA (1997) Global precipitation: a 17-year monthly analysis based on gauge observations, satellite estimates and numerical model outputs. Bull Am Meteorol Soc 78:2539–2558. doi:10.1175/1520-0477(1997)078<2539:GPAYMA>2.0.CO;2

Yoshioka M, Mahowald NM, Conley AJ, Collins WD, Fillmore DW, Zender CS, Coleman DB (2007) Impact of desert dust radiative forcing on Sahel precipitation: relative importance of dust compared to sea surface temperature variations, vegetation changes and greenhouse gas warming. J Clim (submitted)

Zeng N, Neelin JD, Lau KM, Tucker CJ (1999) Enhancement of interdecadal climate variability in the Sahel by vegetation interaction. Science 286:1537–1540. doi:10.1126/science.286.5444.1537

Zhang R, Delworth TL (2006) Impact of Atlantic multidecadal oscillations on India/Sahel rainfall and Atlantic hurricanes. Geophys Res Lett 33:17712. doi:10.1029/2006GL026267